Retrieving Snow Depth Information From AMSR2 Data for Qinghai–Tibet Plateau

Jianshun Wang, Xiaodong Huang, Yunlong Wang, and Tiangang Liang

***Abstract*—Passive microwave data have been extensively used for snow depth (SD) inversion, but their accuracy has large error in the Qinghai–Tibet Plateau (QTP). Thus, there is still room for improvement in regional SD inversion. Ground-measured SD data combined with elevation, longitude, and land cover data were used to develop a multifactor SD inversion model based on Advanced Microwave Scanning Radiometer 2 (AMSR2) over the QTP. The SD inversion model and the AMSR2 SD product were validated and compared using the meteorological stations and ground-measured SD over the QTP at the same time. The results show that the root-mean-square error (RMSE) of the novel model developed in this study is approximately 5 cm, which is much better than the accuracy of the AMSR2 SD product (11–13 cm) released by the Japan Aerospace Exploration Agency. When the ground-measured SD is less than 30 cm, the RMSE and the mean absolute error of the developed model are below 7 and 6 cm, respectively, and the BIAS is approximately 1 cm. The SD inversion results are poor in the western part of the plateau due to the complex terrain and thick snow cover, and its RMSE is greater than 15 cm. In conclusion, this novel SD inversion model is more applicable and accurate than the AMSR2 SD products.**

***Index Terms*—Advanced Microwave Scanning Radiometer 2 (AMSR2), multiparameter, Qinghai–Tibet Plateau (QTP), snow depth (SD).**

I. Introduction

SNOW is an important land cover type that plays a critical role in the global water cycle and energy exchange [1], [2]. Snow parameters, such as snow cover extent, snow depth (SD), and snow water equivalent (SWE), are vital for research on regional climate change, water resource utilization, and natural disaster monitoring [2]–[6]. SD is one of the important parameters used to describe snow properties, and it also plays a vital role in snow disaster monitoring and early warning, water resource assessments, hydrological climate simulations, and surface radiation balance [7]–[10]. The Qinghai–Tibet Plateau (QTP) is sensitive to global climate change [11]. Moreover, the QTP acts as a barrier that impacts the ecological security of China and even Asia [12]. In the context of global climate warming, the temperature change over the QTP is significant. Many of the glaciers and perennial snow cover have begun to melt [12], [13]. The seasonal snow extent has not obviously changed in recent years, but the total amount of snow cover has significantly decreased [13]–[18]. The eco-environment of the plateau is continuously worsening. Snowmelt is a key supplementary water source for rivers and lakes [6], [16]. The QTP is the headstream of many rivers in China, which is why it is called Asia's water tower. The QTP is also one of the three major snow-covered regions and important pastoral areas in China. Changes in snow cover are closely related to local agriculture and animal husbandry. Therefore, the study of snow on the QTP is significant for understanding the changes in the regional eco-environment and sustainable development of agriculture and animal husbandry.

Currently, satellite observations are an effective way to monitor snow cover, and passive microwave remote sensing data are extensively used for SD inversion [4], [19]–[21]. Passive microwave remote sensing has the ability to penetrate clouds and rain to make observations in all weather conditions, and it can also penetrate snow cover to obtain radiometric information with high temporal resolution [22], [23]. The Scanning Multichannel Microwave Radiometer (SMMR), Special Sensor Microwave/Imager (SSM/I), Advanced Microwave Scanning Radiometer–Earth Observing System (AMSR-E), and Advanced Microwave Scanning Radiometer 2 (AMSR2) are the main passive microwave data currently used for SD inversion throughout the world [24]. SMMR passive microwave data were used for SD inversion by Chang, who first proposed the brightness temperature gradient for the SD inversion method [25]. This algorithm can be used for large-scale SD inversions, but the inversion result errors are comparatively large over the QTP [7], [26], [27]. A new algorithm (GSFC 1996) based on Chang's algorithm was developed for study areas in North America and Eurasia, and this algorithm considered the influences of forest and snow grain sizes [28]. Tait used SSM/I passive microwave data to invert SD, and study areas in the USA and Russia were divided into different underlying surface types for SD inversion [29]. The inversion results were poor in the areas not covered by forest where wet snow existed. Based on varied ground emissivity, Dai *et al.* utilized multiple remote sensing data to estimate the SD over the QTP, and this study corrects the coefficient of Chang's algorithm [30].

Manuscript received December 16, 2018; revised November 23, 2019 and December 10, 2019; accepted January 20, 2020. Date of publication February 3, 2020; date of current version February 21, 2020. This work was supported in part by the Chinese Natural Science Foundation Projects under Grant 41971293, Grant 41671330, and Grant 41871238, in part by the Science and Technology Basic Resource Investigation Program of China under Grant 2017FY100501, in part by the Program for Changjiang Scholars and Innovative Research Team in University under Grant IRT_17R50, and in part by the Startup Foundation for Introducing Talent of the Nanjing University of Information Science and Technology under Grant 20191017. *(Corresponding author: Xiaodong Huang.)*

J. Wang, Y. Wang, and T. Liang are with the State Key Laboratory of Grassland Agro-Ecosystems, College of Pastoral Agriculture Science and Technology, Lanzhou University, Lanzhou 730000, China (e-mail: wangjsh17@lzu.edu.cn; wangyl15@lzu.edu.cn; tgliang@lzu.edu.cn).

X. Huang is with the School of Geographical Sciences, Nanjing University of Information Science and Technology, Nanjing 210044, China (e-mail: huangxd@lzu.edu.cn).

Digital Object Identifier 10.1109/JSTARS.2020.2970738

This work is licensed under a Creative Commons Attribution 4.0 License. For more information, see http://creativecommons.org/licenses/by/4.0/

At present, the existing global SD products based on various passive microwave radiometers have large errors in the regional scale, especially in the mountainous area [31]–[33]. In recent years, SD inversion algorithms suitable for China have also been researched and explored by Chinese scholars. In a previous study, the landforms in western China were divided into different units, and Chang's algorithm was corrected based on SMMR passive microwave data [34]. The SSM/I passive microwave data were used to invert the SD in China after the scatterers (precipitation, cold desert, and frozen earth) were eliminated, which have scattering characteristics similar to snow, and better accuracy was obtained [8]. AMSR-E passive microwave data were used to develop an SD inversion algorithm that was suitable for Xinjiang, China, based on different snow grain sizes, snow densities, and snow temperatures [1]. Liang *et al.* combined passive microwave data with visible and near-infrared MODIS data and used a support vector machine to invert the SD in northern Xinjiang, China [35]. This method improved the accuracy of SD inversion to a certain extent. An improved AMSR2 SD inversion algorithm based on AMSR2 passive microwave data was established for a study area in northern Xinjiang, China [24], and it was more accurate than the standard AMSR2 SD products. In summary, it can be seen that there are few related studies on SD inversion over the QTP that using AMSR2 passive microwave data.

Compared with other snow-covered areas in the northern hemisphere, the QTP is the unique mid-latitude mountainous snow-covered area with complex terrain. Due to the complex topography and shallow snow cover with severe fragmentation over the QTP, the passive microwave SD products that are widely used in this region have not achieved ideal monitoring accuracies [7], [8]. In the mid-latitude alpine regions, snow cover changes can affect and even dominate the local and regional climate and hydrological processes. Therefore, snow cover changes in mountain areas are currently receiving increased attention from researchers [36]. The previous SD inversion algorithm is still not effective in regional SD inversion, and the numerous SD inversion algorithms are subject to many restrictions and poor precision in the QTP [30]–[32]. Therefore, there is still room for improvement in regional SD inversion. Passive microwave data, such as SSM/I, SMMR, and AMSR-E, were used for SD/SWE inversions, which were designed to operate worldwide for many years [21], [25], [26], [37], [38], but the accuracy of the inversion has proven to be very poor because of coarse resolution (25 km) [38], [39]–[41], especially in mountainous areas such as the QTP [5]. Some snow products, such as GlobSnow, do not even offer data in mountainous areas [39]. Recently, auxiliary factors (i.e., topographic parameters and geographical parameters) were introduced into SD inversion algorithms [22], [42], [43], which improved the accuracy to some extent. The multiple remote sensing data are used in conjunction with passive microwave data to improve the accuracy of SD inversion [35], [44]. Therefore, using only the brightness temperature difference for the inversion SD does not work well. Currently, machine learning algorithms, which produce SD inversion results with high accuracy, have been applied to SD inversions, but its physical mechanism is weak [23]. The Chang algorithm, the GSFC 1996 algorithm, the Savoie algorithm, and the AMSR-E algorithm are semiempirical SD inversion algorithms based on passive microwave data [25], [28], [42], [45]. Therefore, the semiempirical SD inversion algorithm still has certain advantages. Based on the above reasons and the snow characteristics over the QTP, we chose the multilinear regression method to develop a multiparameter model, and inverse SD over the QTP in this article.

AMSR2 is the latest passive microwave sensor. However, the accuracy of AMSR2 SD products over the QTP has not been evaluated to date. Since the snow cover over the QTP is generally shallow and exhibits high spatial heterogeneity, this study first uses the meteorological station and ground-measured SD to evaluate the accuracy of the AMSR2 SD products released by the Japan Aerospace Exploration Agency (JAXA). Then, this study combines the AMSR2 brightness temperature data and other auxiliary data, including the SD data from ground meteorological stations and field-measured data, digital elevation model, longitude, and latitude, to develop a multiparameter SD inversion model over the QTP that using partial SD data to establish an inversion model, and other SD data validate the model. Finally, the accuracy of proposed new model and the sensitivity to land cover, terrain, and SD are evaluated.

II. Study Area and Data

A. Study Area

The QTP (26°00′–39°46′ N, 73°18′–104°46′ E) is located in the southwest of China from the Hengduan Mountains in the East, the Pamirs in the West, the Himalayas in the South, and the Kunlun Mountains–Qilian Mountains in the North, with an area of approximately 2.5 million km^2 (see Fig. 1), which is called Earth's Third Pole and the Roof of the World. It is the world's highest plateau on average, and its average elevation exceeds 4000 m. The QTP is also one of China's three snow-covered areas and an important water source for Asia. The annual average temperature in the coldest parts of the QTP is low (approximately 0 °C), and the average temperature of the warmest month is less than 10 °C [46]. The QTP has many mountains and rivers in its territory, including the Yangtze River, the Yellow River, the Lantsang River, and the Brahmaputra River. The Kunlun Mountains, Qilian Mountains, Tanggula Mountain, the Himalayas, and other mountains are distributed throughout the plateau. The main-land cover types on the plateau are grasslands and bare lands, while other land cover types are relatively scarce. The topography of the area is generally lower in the northeast (approximately 3000 m above sea level) and higher in the southwest (approximately 4000 m above sea level), and the terrain is fragmented. Snow cover on the plateau is generally shallow (approximately 5 cm for most areas in this study period), and snowfall is mostly seasonal [13], [47], [48].

B. AMSR2 Data

AMSR2 brightness temperature data and SD products were acquired from the website of the JAXA.[1] AMSR2 is a new type of sensor that followed AMSR-E, and it is mounted on the

[1] [Online]. Available: https://gcom--w1.jaxa.jp/auth.html

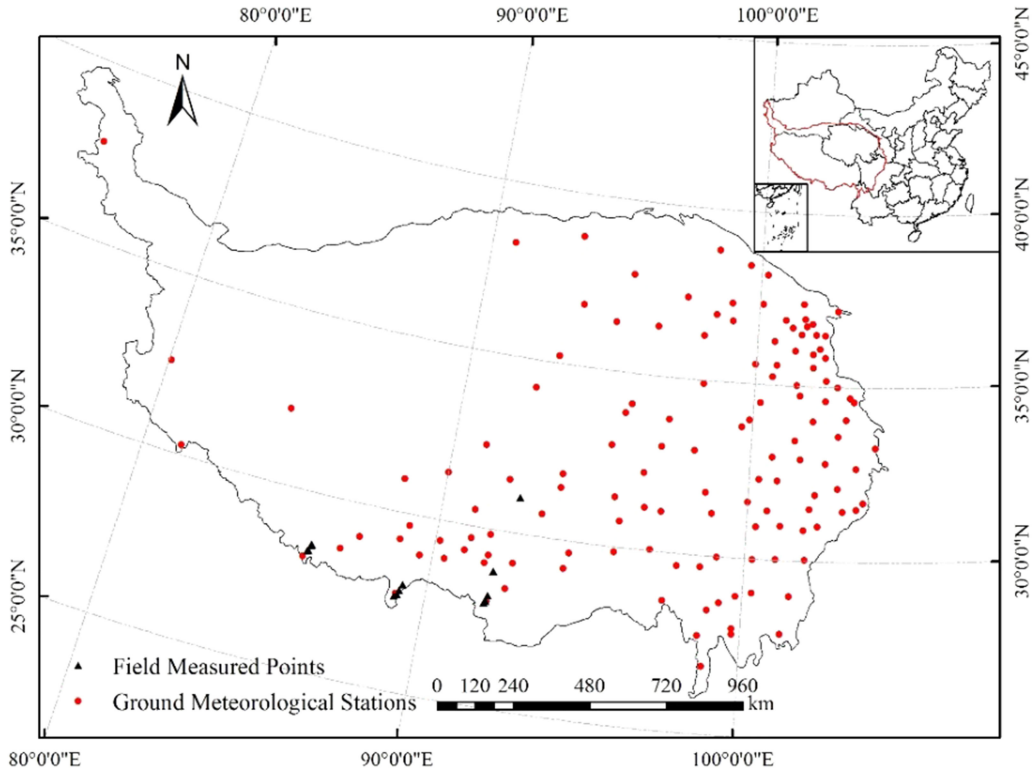

Fig. 1. Ground meteorological stations and field-measured points of the QTP over China.

TABLE I
AMSR2 SENSOR PARAMETERS

Center frequency/GHz	6.9	7.3	10.65	18.7	23.8	36.5	89
IFOV/km^2	35 × 62	35 × 62	24 × 42	14 × 22	15 × 26	7 × 12	3 × 5
Bandwidth/MHz	350	350	100	200	400	1000	3000
Sensitivity/K	0.34	0.43	0.7	0.7	0.6	0.7	1.2

Global Change Observation Mission 1st–Water (GCOM-W1) "SHIZUKU" satellite from Japan. The sensor has 14 channels at seven frequencies: 6.9, 7.3, 10.65, 18.7, 23.8, 36.5, and 89 GHz (see Table I). Each frequency has dual polarization, which are horizontal and vertical. Snowfall on the QTP is mainly concentrated from December to March. Therefore, the brightness temperature data and SD products for the four snow seasons from Dec. 2012 to Mar. 2013, Dec. 2013 to Mar. 2014, Dec. 2014 to Mar. 2015, and Dec. 2015 to Mar. 2016 were selected. Data released and reprocessed by the JAXA have a 10-km resolution, their projection is equirectangular, and their data format is TIFF. The GCOM-W1 satellite has two transit times each day. The transit time of the ascending pass is 13:30 $\pm$ 15 min local time, and the transit time of the descending pass is 01:30 $\pm$ 15 min. According to the analysis of SD data from the ground meteorological stations, the snow cover over the QTP is generally shallow. Therefore, the frequency of 89 GHz, which is sensitive to shallow snow cover, was added to improve the inversion accuracy [45]. The sky radiation and the emission from the intervening atmosphere are small and can be neglected [45], [49]. Therefore, the brightness temperature data from five frequencies of AMSR2 were selected, that is, 10.65, 18.7, 23.8, 36.5, and 89 GHz (hereafter abbreviated as 10, 18, 23, 36, and 89 GHz).

C. Ground Observation Data

The data from 133 meteorological stations used in this article were provided by the China National Meteorological Science Data Sharing Service.[2] These data include seven primary components: station number, observation date, longitude, latitude, elevation, daily SD, and daily snow pressure. The field-measured data include 13 sampling sites from March 1 to March 8, 2018 (see Fig. 1). The sample measurement parameters mainly include SD, SWE, snow density, and liquid water content of snow.

The presence of a large water body near the meteorological station will seriously affect the SD inversion [14], [24]. Therefore, the SD from the ground meteorological stations data

[2][Online]. Available: http://data.cma.cn/site/index.html

that were affected by a body of water was not used for model establishment. The pixel of water body was removed before SD inversion. Cold desert, frozen ground, and precipitation have scattering characteristics that are similar to snow cover [43], [50]–[53]. Therefore, the SD data affected by scatterers were also not used for the establishment of SD inversion models.

D. MODIS Data

Snow cover redistribution and microwave radiation are affected by different land cover types [50], [54]. Therefore, different land cover types affect the accuracy of SD inversion. MCD12Q1 is a yearly land cover classification product that is composite data based on one-year MODIS Earth observation. This product has five different classification schemes, and supervised classification is the main classification technique used for this product. The land-cover-type product with a spatial resolution of 500 m in 2014 was used in this article based on the International Geosphere-Biosphere Program (IGBP) classification system. This product contains a total of 17 land cover types with 11 natural vegetation types, three land use and land mosaic types, and three nonvegetation land types [55], [56]. This study referred to the reclassification schemes in [55] and [56] to reclassify MCD12Q1 IGBP into seven categories: water, forests, shrublands, grasslands, farmlands, bare lands, and snow/ice. As AMSR2 passive microwave data are greatly affected by land cover, the reclassified land cover products were used to analyze the influence of different land cover types on the SD inversion accuracy to ensure the accuracy of the model. The land cover dataset on the QTP indicated that grasslands accounted for 56.9% followed by bare lands (29.6%).

The inversion results of land surface parameters would be affected by microwave radio emissivity indirectly. Therefore, the Collection-6 MODIS land surface temperature products were used to obtain ground emissivity, which were resampled to 10-km spatial resolution consistent with AMSR2. The MODIS snow products of collection 5 (MYD10A1 and MOD10A1) was used to identify the snow cover optically. The snow cover with no cloud was developed by Wang *et al.* [56], which was used to extract snow cover area and no snow cover area.

III. Methodology

A. Factors Screening

The upwelling radiation observed as the apparent temperature at a satellite microwave radiometer (T_b) can be expressed as [45], [49]

$$T_b = (RT_{\rm sky} + (1 - -R)\, T_{\rm surf})\, e^{--t} + T_{\rm atm} \qquad (1)$$

where e^{-t} is the atmospheric transmissivity, R is the surface reflectivity, $T_{\rm sky}$ is the sky radiation, $T_{\rm surf}$ is the surface emission, and $T_{\rm atm}$ is the atmospheric component. In general, $T_{\rm atm}$ and $T_{\rm sky}$ are neglected as they are small [45], [49].

SD and snow grain have an effect on the scattering of microwave radiation [25]. Namely, as the SD increases, the effect of snow grain scattering of the microwave radiation strengthens; therefore, the less microwave energy reaches the sensor, and the value of the brightness temperature decreases [57], [58]. The high-frequency channels usually have stronger scattering effects on snow than the low-frequency channels. Therefore, the brightness temperature of snow is lower in the high-frequency channel than in the other channels. The vertical polarization brightness temperature is higher than the horizontal polarization brightness temperature under the same conditions, and the microwave radiation response of horizontal polarization to snow is more sensitive than that of vertical polarization (see Table II). The sensitivity of the radiation brightness temperature to SD becomes weak when the SD reaches a certain value; this phenomenon occurs because the SD becomes deep enough that the radiation is poorly reflected, which limits the ability of the sensors to detect the microwave emission [9], [51]. In the Chang algorithm, SD is closely correlated with the brightness temperature data at 19 and 37 GHz. The Chang algorithm cannot invert SD very well in areas with shallow snow cover. Some researchers have applied 89- and 23-GHz data to snow cover detection and SD inversion [6], [23], and we added 23-GHz data to inverse the SD. Because the snow cover over the QTP is generally shallow, 89 GHz was added to the inversion model to invert shallow SD, and 10 GHz was used to invert thick SD [45]. Because the ascending data were affected by wet snow in the day time, only the descending data of AMSR2 from the four snow season were analyzed here.

As shown in Table II, vertical channels of 10 and 18 GHz are relatively insensitive to changes in SD, 36 GHz is the most sensitive, and the other channels exhibit limited differences in sensitivity to SD changes. The five frequency channels selected in this article are significantly correlated with SD. The results of the correlation matrix between channels are shown in Table III, where the correlation coefficients between most channels are above 0.5, and the correlation coefficient between only 89 and 10 GHz is below 0.5. Between some channels, the correlation coefficient even exceeds 0.9, such as between 10H and 18H, 10V and 18V, 18H and 18V, 18H and 23H, 18H and 23V, 18V and 23H, 18V and 23V, 23H and 23V, 23H and 36H, 36H and 36V, and 89H and 89V.

Elevation, slope, aspect, wind speed, and wind direction are the main factors that affect the distribution of snow cover [27], [37], [47], [59], [60]. As the elevation increases, the temperature decreases, the snow cover melts slowly, and the liquid water content in the snow cover decreases. Consequently, terrain changes have an effect on SD. The terrain parameters (elevation, slope, and aspect) and geographic parameters (latitude and longitude) were used for SD inversion and SWE estimation [22], [52]. Therefore, elevation was used as a parameter to construct an SD inversion model in this article.

When Tait [29] inverted the SD over the USA and Russia, he found that the inversion results of the forest-covered area were poor. Forests had a greater impact on the SD inversion because it contributed a lot of microwave radiation [21], [26]. Because the forest accounts for only approximately 7% of the QTP according to MCD12Q1 and the meteorological stations are sparsely distributed in the forest, the forest would not have much impact on the SD inversion of the QTP. Grasslands cover nearly 60% of the QTP according to MCD12Q1. Grassland is a

TABLE II
CORRELATION AND SENSITIVITY OF EACH CHANNEL TO THE MEASURED SD OF ALL STUDY PERIOD

Frequency channel	One–way regression equation	Sensitivity (or slope)	Correlation (r)
10H	Y = –0.442*x+249.43	–0.442	–0.427**
10V	Y = –0.293*x+257.04	–0.293	–0.409**
18H	Y = –0.517*x+246.74	–0.517	–0.477**
18V	Y = –0.388*x+254.89	–0.388	–0.457**
23H	Y = –0.531*x+246.12	–0.531	–0.465**
23V	Y = –0.409*x+253.04	–0.409	–0.435**
36H	Y = –0.607*x+239.63	–0.607	–0.401**
36V	Y = –0.547*x+245.65	–0.547	–0.384**
89H	Y = –0.490*x+224.22	–0.490	–0.220**
89V	Y = –0.448*x+229.35	–0.448	–0.207**

Note: "**"represents a significant correlation at the 0.01 level (two-tail), *Y* represents the corresponding frequency channel, and *x* represents the measured SD from meteorological stations and ground measured.

TABLE III
CORRELATION MATRIX BETWEEN SD AND EVERY CHANNEL

	SD	10H	10V	18H	18V	23H	23V	36H	36V	89H	89V
SD	1										
10H	–0.427**	1									
10V	–0.409**	0.835**	1								
18H	–0.477**	***0.925*****	0.872**	1							
18V	–0.457**	0.859**	***0.907*****	***0.947*****	1						
23H	–0.465**	0.885**	0.840**	***0.981*****	***0.946*****	1					
23V	–0.435**	0.812**	0.849**	***0.928*****	***0.973*****	***0.962*****	1				
36H	–0.401**	0.718**	0.686**	0.855**	0.844**	***0.915*****	***0.907*****	1			
36V	–0.384**	0.662**	0.665**	0.804**	0.836**	0.873**	***0.906*****	***0.984*****	1		
89H	–0.220**	***0.419*****	***0.384*****	***0.525*****	***0.476*****	***0.588*****	***0.549*****	0.738**	0.706**	1	
89V	–0.207**	***0.383*****	***0.360*****	***0.490*****	***0.458*****	***0.556*****	***0.533*****	0.720**	0.702**	***0.992*****	1

Note: "**"represents significance at the 0.01 level of correlation (two-tail).

low-vegetation cover area, and the scattering of microwaves is much less than that of forests [23]. Therefore, this study considered only the influence of grasslands to establish an SD inversion algorithm.

As shown in Table IV, the correlations between brightness temperature difference and longitude, latitude, and elevation were all low. This result indicates that using only the brightness temperature difference or another single variable cannot achieve ideal SD inversion results.

Multifactor regression models were used for SD inversion in this study. The multifactor regression model can be expressed as follows:

$$y_i = \alpha + \beta_1 x_1 + \beta_2 x_2 + \ldots + \beta_k x_k + \varepsilon_j \quad (2)$$

$$y_i = \alpha + \beta_1 \ln x_1 + \beta_2 \ln x_2 + \cdots + \beta_k \ln x_k + \varepsilon_j \quad (3)$$

$$y_i = \alpha + \beta_1 \frac{1}{x_1} + \beta_2 \frac{1}{x_2} + \cdots + \beta_k \frac{1}{x_i} + \varepsilon_j \quad (4)$$

where y_i is the dependent variable, x_1, x_2, x_3, …, x_k are independent variables, β is the regression coefficient, and ε_j is the error term. If there is a linear relationship between x_1 and x_2

TABLE IV
CORRELATION MATRIX BETWEEN THE BRIGHTNESS TEMPERATURE DIFFERENCE AND LONGITUDE, LATITUDE, AND ELEVATION

Independent variables	Longitude	Latitude	Elevation
10H36H	–0.077**	–0.081**	0.012
10H36V	–0.078**	0.006	–0.099**
10H89H	–0.023	0.059*	0.132**
10H89V	–0.020	0.095**	0.090**
10V36H	–0.061**	–0.268**	0.167**
10V36V	–0.067**	–0.198**	0.067**
10V89H	–0.017	–0.050*	0.217**
10V89V	–0.015	–0.015	0.178**
18H89H	–0.009	0.075**	0.151**
18H89V	–0.006	0.114**	0.105**
18V89H	–0.013	–0.017	0.230**
18V89V	–0.011	0.020	0.189**
23H89H	0.001	0.082**	0.154**
23H89V	0.003	0.123**	0.106**
23V89H	–0.004	–0.007	0.230**
23V89V	–0.002	0.032	0.188**
36H89H	0.023	0.135**	0.169**
36H89V	0.026	0.184**	0.112**
36V89H	0.168**	0.450**	–0.155**
36V89V	0.143**	0.497**	–0.215**

Note: "**"represents significance at the 0.01 level of correlation (two-tail). "10H36H" represents the combination of 10 and 36 H; the others are the same.

(or other independent variables), then

$$x_1 = c + dx_2. \tag{5}$$

This situation is called multicollinearity between independent variables. For this reason, it is impossible to separate the influence of an independent variable on the dependent variable while controlling another independent variable [61]. In other words, if there is a strong correlation between the channels, one channel will be able to almost completely or completely replace another channel, making use of the brightness temperature difference meaningless. If x_1 and x_2 have multicollinearity, these two independent variables will not be included in the same model, as well as brightness temperature difference. Therefore, a combination of brightness temperature differences with low correlation between every channel was added to the SD inversion model in this article, and a more accurate and reliable inversion model was constructed.

B. Scatterer Screening and Snow Identification

Cold desert, frozen ground, and precipitation have scattering characteristics that are similar to snow cover [50]–[53]. In general, the polarization difference progressively increases as one views bare soils, snow-covered fields, deserts, and water surfaces [43]. The polarization difference for melting snow is nearly the same as dry snow, although the scattering signature decreases significantly due to melting [51]. Kelly [45] eliminated the effects of these scatterers to improve the inversion accuracy based on the research by Grody and Basist [52], and AMSR-E passive microwave data were used to establish an SD inversion model [45], [51]. AMSR-E data have frequency channels that are similar to the AMSR2 channels, so Kelly's method was used to eliminate the effects of scatterers in this study. To improve the accuracy of the SD inversion algorithm, the impacts of cold desert, frozen ground, and precipitation scatterers were eliminated before the SD inversion model was established. In

addition, the presence of wet snow also affects SD inversion [42], [45], and Walker's method was used to remove the influence of wet snow [51]. The removal methods of Grody, Kelly, and Walker are as follows:

1) scattering signature: 18V – 36V $>$ 0 K;
2) precipitation: 23V $\geq$ 259 K or 254 K $\leq$ 23V $\leq$ 258 K and 18V – 36V $\leq$ 2 K;
3) cold desert: 18V – 18H $\geq$ 18 K and 18V – 36V $\leq$ 10 K and 36V – 89V $\leq$ 10 K;
4) frozen ground: 18V – 18H $\geq$ 8 K and 18V – 36V $\leq$ 2 K and 23V – 89V $\leq$ 6 K;
5) wet snow: 36V – 36H $\geq$ 10 K.

C. Accuracy Evaluation

The *k*-fold cross-validation was used to model establish and evaluate the accuracy of the model for many studies [63], and the tenfold cross-validation was used in this study. The coefficient of determination (R^2) and root-mean-square error (RMSE) of the validation set strongly determine the model accuracy, and higher R^2 and lower RMSE represents the high accuracy of the model.

The SD data from the ground meteorological stations and the field-measured data were used as true values to evaluate the accuracy of ascending SD products, descending SD products, and the SD inversion model. Compared with the selected AMSR2 SD products, the model with small RMSE, mean absolute error (MAE), and bias (BIAS) values was chosen as the optimal SD inversion model in this article. The measured SD, elevation, latitude, longitude, and underlying surface were used to evaluate and analyze the accuracy of each model. Finally, an optimal inversion model was obtained. The accuracy evaluation criteria are as follows:

$$R^2 = 1 - \frac{\sum_{i=1}^{n} \left(\mathrm{SD}_0 - \mathrm{SD}_x\right)^2}{\sum_{i=1}^{n} \left(\mathrm{SD}_x - \overline{\mathrm{SD}_0}\right)^2} \tag{6}$$

$$\mathrm{RMSE} = \sqrt{\frac{1}{n} \sum_{i=1}^{n} \left(\mathrm{SD}_0 - \mathrm{SD}_x\right)^2} \tag{7}$$

$$\mathrm{MAE} = \frac{1}{n} \sum_{i=1}^{n} \left|\mathrm{SD}_0 - \mathrm{SD}_x\right| \tag{8}$$

$$\mathrm{BIAS} = \frac{1}{n} \sum_{i=1}^{n} \left(\mathrm{SD}_0 - \mathrm{SD}_x\right) \tag{9}$$

$$\mathrm{MRE} = \frac{1}{n} \sum_{i=1}^{n} \left(\frac{\left|\mathrm{SD}_0 - \mathrm{SD}_x\right|}{SD_0}\right) 100\% \tag{10}$$

where SD_0 and SD_x represent the measured SD and the inversion SD, respectively, and n is the number of samples used for evaluation.

D. SD Inversion Method

A linear relationship is observed between SD and brightness temperature differences when the snow grain size is constant [25], [62]. This article introduced the elevation, latitude, and longitude of the meteorological stations into the SD inversion to improve the accuracy of the model and construct a novel multiple linear regression model. The brightness temperature (Tb), the brightness temperature difference (TBD), the natural logarithm of the brightness temperature (lnTb), and the reciprocal of brightness temperature (reTb) were used to established the multifactor model as an independent variable. Then, the independent variables that passed the *F* test will be used to develop a multifactor SD inversion model. The different combinations of elevation, latitude, longitude, TB, TBD, lnTB, and reTB would be introduced to retrieve SD over the QTP.

IV. Results and Analysis

A. Evaluation of the Accuracy of AMSR2 SD Products

The SD data from the ground meteorological stations and field-measured data were assumed to be the true values, and the accuracies of the ascending and descending AMSR2 SD products were evaluated. The ascending AMSR2 SD product has a smaller RMSE (11.82 cm) than the descending product. However, the difference between them is only 1.52 cm. In addition, the average SD of the descending product is 4.73 cm, which is closer to the measured average SD (5.30 cm), and it has a smaller BIAS (0.57 cm) with less underestimation of the SD than the ascending product (see Table V). The average SD of the ascending product is 0.67 cm, which has a larger BIAS (4.60 cm) and is different from the measured average SD of 5.30 cm. This result shows that the descending AMSR2 SD product has better accuracy than the ascending product over the QTP. Moreover, due to the effect of snowmelt during the transit time of the ascending product, the liquid water in the snow will affect the SD inversion [53]. Therefore, the descending product was selected in this study for the establishment of an SD inversion model.

The AMSR2 official algorithm is briefly described as follows. If Tb89V $<$ 255 K, Tb89H $<$ 255 K, Tb23V $>$ Tb89V, Tb23H $>$ Tb89H, and T $<$ 267 K is satisfied, the snow cover is shallow, and the SD is set to 5.0 cm; if Tb36H $<$ 245 K and Tb36V $<$ 255 K, the snow cover is identified as moderate to deep snow. Calculating SD for moderate to deep snow cover is as follows:

$$\begin{aligned}\mathrm{SD} = {} & \left[1/\log_{10}\left(\mathrm{Tb36V} - \mathrm{Tb36H}\right) * \left(\mathrm{Tb10V} - \mathrm{Tb36V}\right)\right] \\ & + \left[1/\log_{10}\left(\mathrm{Tb18V} - \mathrm{Tb18H}\right) * \left(\mathrm{Tb10V} - \mathrm{Tb18V}\right)\right]\end{aligned} \tag{11}$$

For other details, refer to [24] and [45].

B. Multiparameter SD Inversion Model

The frequencies of 89 and 10 GHz were added to invert shallow and deep snow cover, respectively. Different combinations of Tb, TBD, lnTb (natural logarithm of brightness temperature), reTb (reciprocal of brightness temperature), elevation, longitude, and latitude were used to construct a multifactor regression model for SD inversion. From Table VI, R^2 for each model validation set is between 0.51 and 0.62, and the RMSE

TABLE V
COMPARISON OF THE ACCURACY OF THE ASCENDING AND DESCENDING AMSR2 SD PRODUCTS OVER THE QTP

AMSR2 SD products	Measured average SD (cm)	Average SD of snow products (cm)	RMSE (cm)	BIAS (cm)	MAE (cm)
Descending	5.30	4.73	13.34	0.57	7.26
Ascending		0.67	11.82	4.60	5.28

TABLE VI
SD INVERSION MODEL AND INVERSION ERROR

Model	Training set		Validation set	
	R^2	RMSE (cm)	R^2	RMSE (cm)
M1	0.53**	6.19	0.51**	6.21
M2	0.55**	5.99	0.59**	5.39
M3	0.53**	6.07	0.57**	5.53
M4	0.54**	6.02	0.59**	5.41
M5	0.55**	5.97	0.59**	5.37
M6	0.59**	5.67	0.62**	5.24
M7	0.60**	5.64	0.62**	5.21
M8	0.60**	5.62	0.61**	5.31

Note: "**"means the model passed the F test at $P < 0.001$.

is between 5.21 and 6.21. The results of the analysis show that the introduction of 23 GHz can improve the accuracy of the SD inversion over the QTP. The introduction of brightness temperature differences between 10 and 89 GHz can also improve the inversion accuracy. The first four models have lower accuracy compare to the other three. Therefore, the last three models are evaluated and analyzed its accuracy hereinafter.

The specific formulas of eight models are listed as follows:

$$SD_{M1} = 112.2 - 0.402\,(La) - 0.857\,(Lon) - 4.702 \times 10^{-3}\,(Ele) - 1.256\,(Tb10H - Tb36H) + 0.968\,(Tb10H - Tb36V) + 0.262\,(Tb10H - Tb89H) + 0.33\,(Tb10V - Tb36H) - 1.366\,(Tb23H - Tb89H) + 1.121\,(Tb23V - Tb89H)$$

$$SD_{M2} = -263 - 0.328\,(La) - 1.003\,(Lon) - 4.522\times10^{-3}\,(Ele) + 170.4\,\ln(Tb10V) - 336.6\,\ln(Tb23H) + 259.1\,\ln(Tb23V) + 196.4\,\ln(Tb36H) - 219.8\,\ln(Tb36V)$$

$$SD_{M3} = 107.1 - 0.345\,(La) - 0.846\,(Lon) - 0.004\,(Ele) - 0.339\,(Tb10H–Tb10V) + 1.309\,(Tb10H - Tb23H) - 0.935\,(Tb10H - Tb23V) - 0.825\,(Tb10H - Tb36H) + 0.876\,(Tb10H - Tb36V)$$

$$SD_{M4} = 57.03 - 0.38\,(La) - 1.045\,(Lon) - 0.005\,(Ele) + 0.714\,(Tb10V) - 1.346\,(Tb23H) + 0.962\,(Tb23V) + 0.709\,(Tb36H) - 0.761\,(Tb36V)$$

$$SD_{M5} = 219.2 - 0.389\,(La) - 1.043\,(Lon) - 0.005\,(Ele) - 4.837\times10^{4}\,(1/Tb10V) + 5.733\times10^{4}\,(1/Tb23H) - 3.222\times10^{4}\,(1/Tb23V)$$

$$SD_{M6} = 271 - 0.72\,(Lon) - 1.789\times10^{-3}\,(Ele) - 1.906\,(Tb10H) + 17.18\,(Tb23H) - 0.15\,(Tb23V) - 1.383\times10^{5}\,(1/Tb10H) + 1.093\times10^{6}\,(1/Tb23H) - 1.018\times10^{6}\,(1/Tb23V)$$

$$SD_{M7} = 2.947\times10^{3} - 0.712\ Lon - 1.658\times10^{-3}\ Ele + 0.359\ Tb10H + 32.47\ Tb23H - 28.75\ TbTb23V - 4.228\times10^{-2}\ Tb89V - 8.195\times10^{3}\ \ln(Tb23H) + 7.492\times10^{3}\ \ln(Tb23V)$$

$$SD_{M8} = -1.611\times10^{3} - 0.748\ Lon - 2.085\times10^{3}\ Ele - 37.93\,(Tb10H - Tb23H) + 31.26\,(Tb10H - Tb23V) + 0.836\,(Tb10H - Tb89V) + 1.502\times10^{3}\ \ln(Tb10H) - 9.505\times10^{3}\ \ln(Tb23H) - 8.135\times10^{3}\ \ln(Tb23V) + 173.6\ \ln(Tb89V).$$

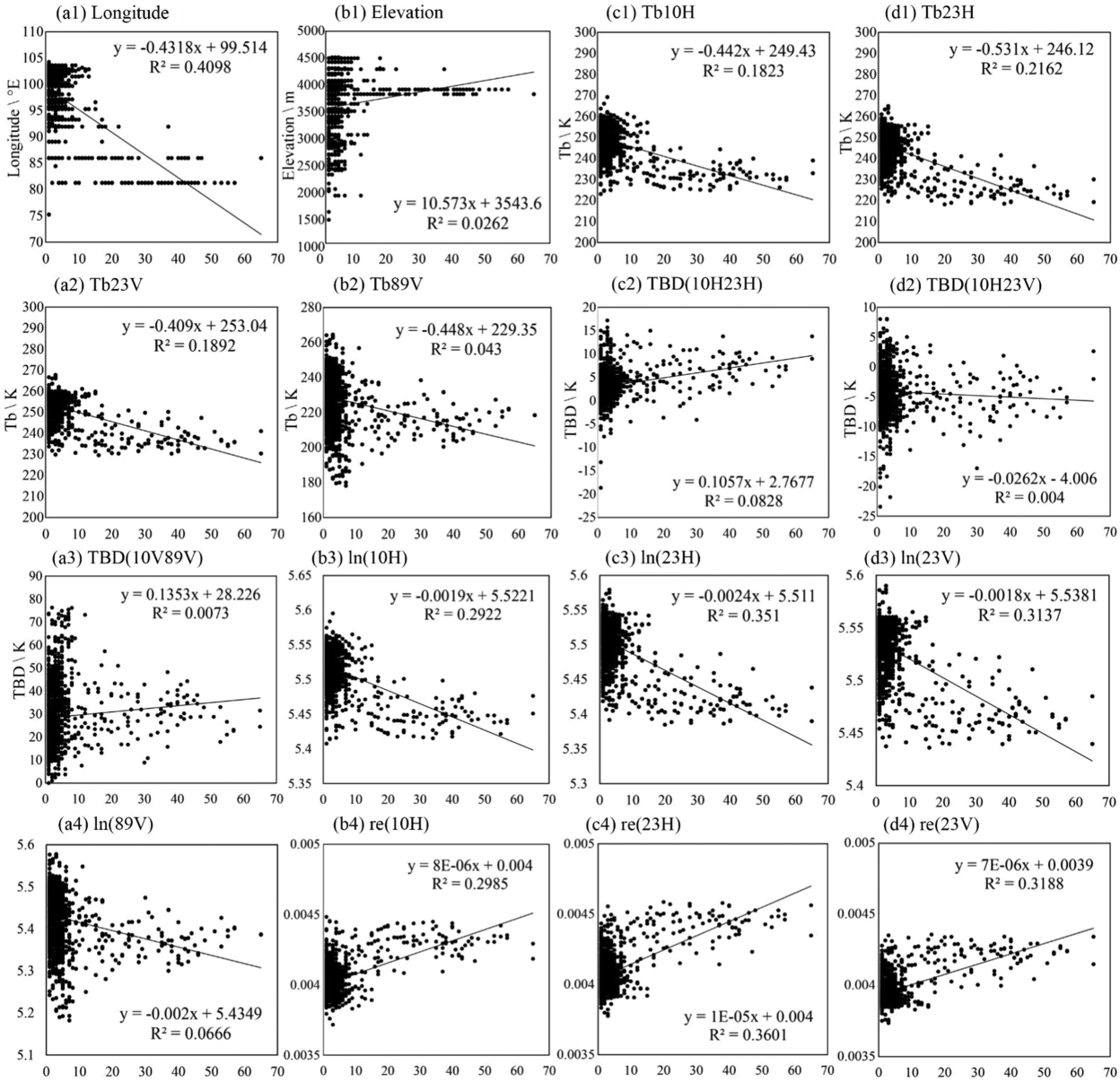

Fig. 2. Scatter map of each coefficient with the SD for M6, M7, and M8, where *ln* and *re* represents the natural logarithm and the reciprocal, respectively, for corresponding parameters. The units of elevation, brightness temperature (Tb), and brightness temperature difference (TBD) are *m, K,* and *K,* respectively. There are no units for the natural logarithm of Tb and the reciprocal of Tb.

In the formula, Ele is the elevation; La is the latitude; Lon is the longitude; 10, 23, 36, and 89 are the frequencies corresponding to AMSR2; V is the vertical channel; and H is the horizontal channel. The units for SD, elevation, and brightness temperature are *cm, m,* and *K*, respectively.

As shown in Fig. 2, longitude has the highest R^2 with 0.4098, and re(23H) is second. The reciprocal of single brightness temperature has generally higher R^2 compared with others. Elevation exhibits weak positive trend with SD for meteorological station over the QTP. The vertical channel of 89 GHz has a small R^2 compared with other three (10H, 23H, and 23V). When retrieval SD in an area with complex terrain as the QTP, the introduction of longitude and reciprocal of single brightness temperature (re10H, re23H, and re23V) for the multifactor inversion model have better performance compared with AMSR2 descending SD products.

C. Accuracy Comparison

The RMSE, MAE, and BIAS of each SD inversion model are smaller than those of the descending AMSR2 SD product, and the inversion accuracies of all models are significantly improved (see Fig. 3). However, the SD inversion model in this article exhibits a certain underestimation of thick snow cover. The inversion results of the descending AMSR2 SD product have a large error for the measured SD, which is greater than 10 cm, and the inversion results of some measured SDs that larger than 30 cm are even 0 cm. Compared with the SD inversion model in

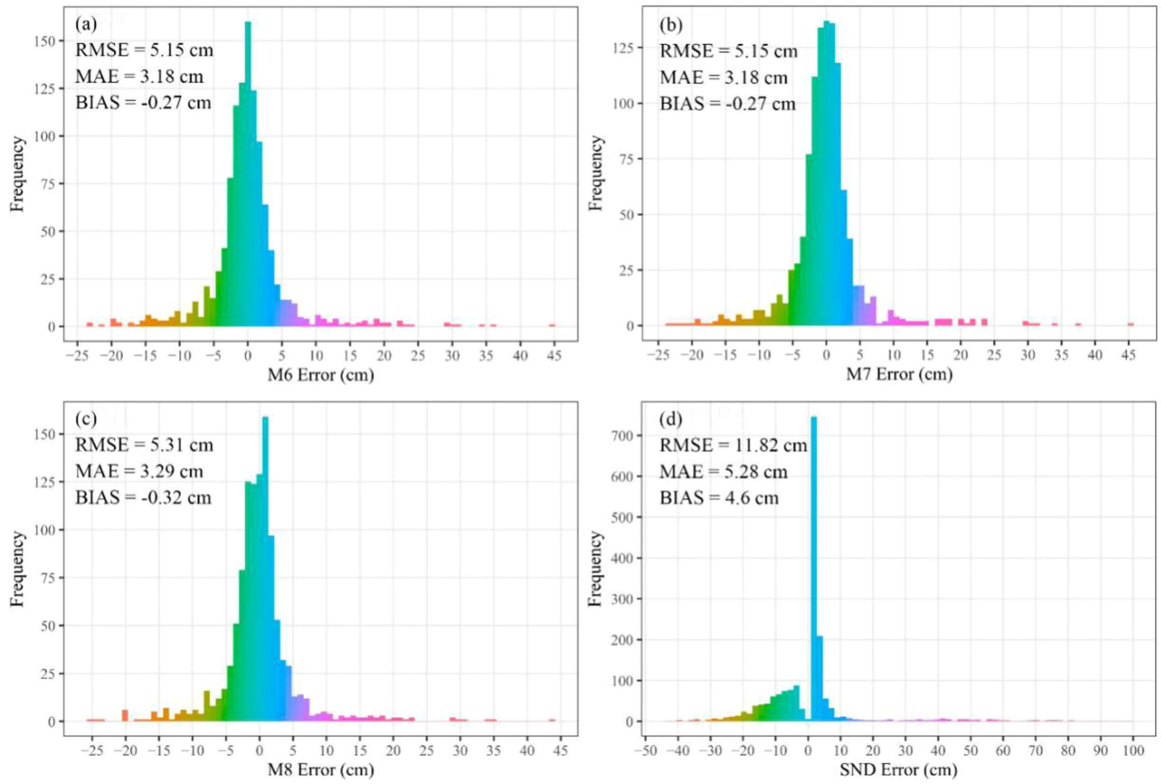

Fig. 3. Error frequency distribution of retrieved SD and AMSR2 descending SD, where SND is the descending SD product of AMSR2. The error is equal to the measured SD minus the retrieved SD. (a) M6. (b) M7. (c) M8. (d) AMSR2.

this study, the accuracy of the descending AMSR2 SD product is poor and seriously underestimates the SD of some regions over the QTP. In addition, the SD product seriously overestimates the SD that less than 10 cm. The research results show that the AMSR2 SD product that is applicable to most of the world is a set of SD products based on the global SD inversion model. However, for the QTP, this product has poor accuracy and cannot accurately reflect the spatial distribution properties of SD.

D. Effect of SD on the SD Inversion Accuracy

The study by Markus and Zhang shows that a saturation phenomenon would occur in the brightness temperature differences between 18 and 10 GHz (or 36 GHz) when the measured SD exceeded 30 cm [9], [45], [58]. When the measured SD is greater than 30 cm, the RMSE, MAE, and BIAS of each model were larger (see Table VII). The error of M7 is the largest, and M8 has the smallest error, which is relatively suitable for the inversion of thick snow cover. When the measured SD is less than 30 cm, the RMSE, MAE, and BIAS are small for all models, and the RMSE is less than 7 cm. This result shows that the accuracy is poor when the SD inversion model retrieves a measured SD, which is greater than 30 cm. When the SD is less than 30 cm, the three models have a slight underestimation. M8 performs better when the measured SD is less than 30 cm. The combination between TBD and lnTb may be more suitable to retrieve thick snow cover. In a word, M8 has well stability and more accurate inversion results over the QTP.

E. Effect of Terrain on the SD Inversion

The inversion error on SD is smallest in the eastern part of the QTP, and the western part has a maximum inversion error (see Figs. 4 and 5). A large number of ground meteorological stations are concentrated in the central and eastern parts of the plateau, accounting for approximately 97% of the meteorological stations on the plateau. However, the shortage of stations in the western part of the plateau results in relatively large errors for this area. The SD inversion errors are smallest when the elevation of the meteorological station is below 2800 m; in particular, the RMSE for the eastern part and the regions less than 3800 m above sea level is less than 3 cm, and their MREs are the minimum. The SD inversion errors are largest in the areas with elevations above 3800 m; however, the RMSE of the models are relatively smaller in this area, which are less than 9 cm. Approximately 71% of the stations over the QTP are located at less than 3800 m above sea level, and the inversion results are the most accurate at these stations. The analysis of the station data indicates that the ground meteorological stations at elevations above 3800 m have large SD and limited station distribution during the study period, resulting in large inversion errors for each model.

F. Effect of Land Cover Types on the SD Inversion

The inversion results are worst over shrublands, followed by bare lands. Forests, grasslands, and farmlands have significantly smaller inversion errors than shrublands (see Figs. 6 and 7).

TABLE VII
INFLUENCE OF SD ON SD INVERSION

SD	M6			M7			M8		
	RMSE (cm)	MAE (cm)	BIAS (cm)	RMSE (cm)	MAE (cm)	BIAS (cm)	RMSE (cm)	MAE (cm)	BIAS (cm)
< 30 cm	6.72	5.38	1.29	6.61	5.29	1.19	6.66	5.31	0.9
> 30 cm	17.47	15.48	15.47	17.51	15.53	15.53	16.88	14.93	14.9

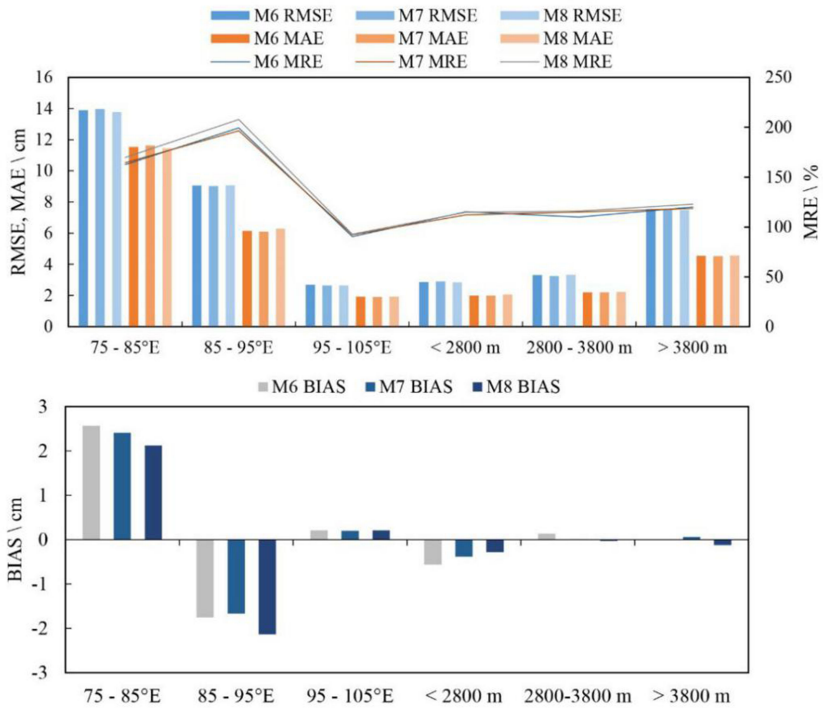

Fig. 4. Influence of elevation and longitude on SD inversion.

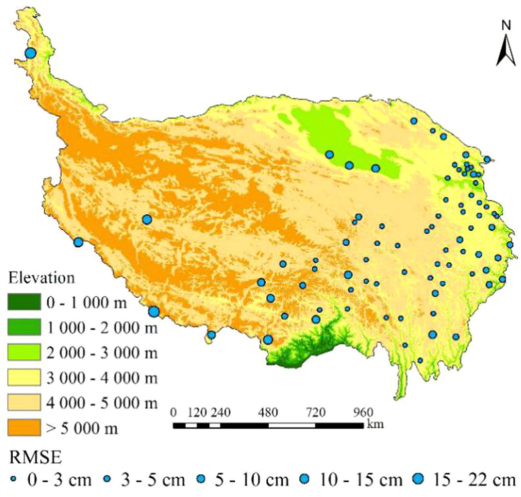

Fig. 5. Meteorological station inversion errors at different elevations and longitudes.

The inversion error of bare lands is second only to shrublands due to the lack of meteorological stations in bare lands. Most of the bare lands are distributed in the inaccessible western part of the QTP, and meteorological data are difficult to obtain from these areas. Grasslands have better SD inversion accuracy, which accounts for more than half of the QTP (for all models, the RMSE is approximately 7 cm, and the MAE is less than 5 cm). Grasslands and farmlands with low vegetation cover have less of a scattering effect on microwave frequencies, which results in reduced inversion error. The verification points over grasslands account for more than 52% of all verification data. There are relatively fewer meteorological stations in forests and shrublands than in grasslands and farmlands, and the snow cover is shallow near meteorological stations in forests. The inversion results are accurate for the shallow snow cover areas in this article. Therefore, the SD inversion model established in this article is applicable to most areas of the QTP.

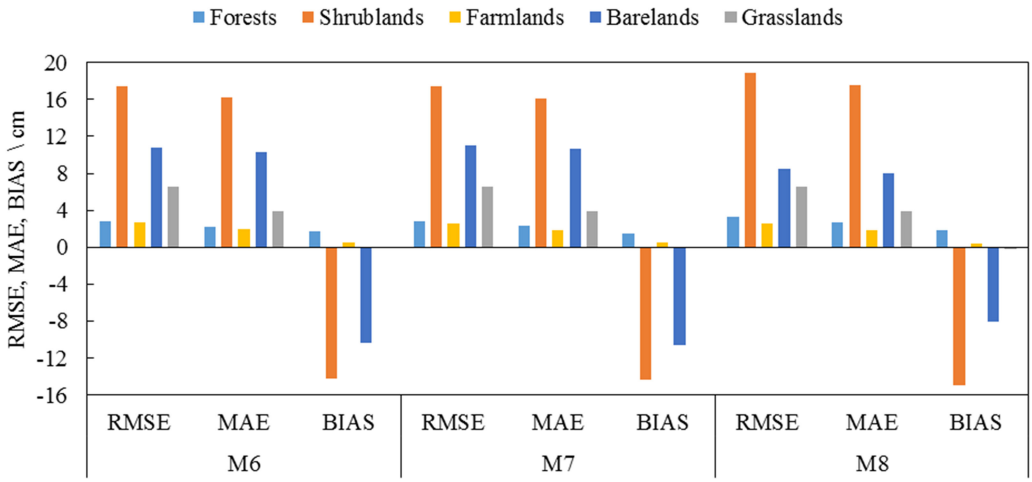

Fig. 6. Influence of different land cover types on the SD inversion.

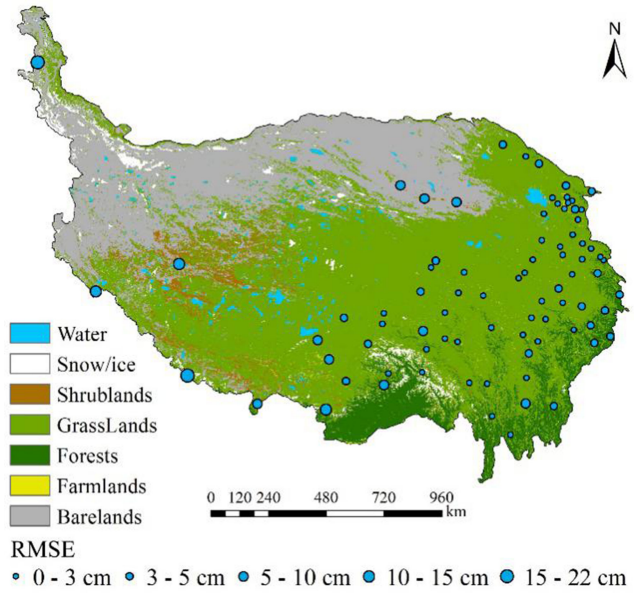

Fig. 7. Meteorological station inversion errors at different land cover types.

G. Optimal Model

Compared with the AMSR2 SD product, the accuracies of all SD inversion models established in this article improved significantly. The introduction of elevation and longitude in the model can effectively improve the accuracy of SD inversion. Under the influence of the measured SD, elevation, longitude, latitude, and land cover type, M8 performed well compared to M6 and M7. M8 had a well R^2 (0.61) and RMSE (5.31 cm). Moreover, M8 is stable to retrieve shallow snow cover and thick snow cover.

The pixel affected by scatterers (cold desert, frozen ground, and precipitation) were removed from the M8 SD maps. Based on original M8 SD maps, the snow-free pixels were eliminated by MODIS cloud-free snow cover products [see Fig. 8(b1)–(b4)]. As shown in Fig. 8(a1)–(a4), the SDs are generally deep in the west and shallow in the east of the plateau. The Pamirs, Kunlun Mountains, Himalayas, and Tanggula Mountains are the main regions with thick snow cover. The descending AMSR2 SD products identified most areas of the plateau as snow-free areas, which caused large errors. Compared to SD maps identified by cloud-free snow cover products, the M8 has a little deviation in identifying snow cover. Although this novel model exhibited slight errors in some regions over the QTP, the above results are similar as the SD distribution characteristics reported by Bai and Che [47], [37], which has more accurate results than AMSR2 SD products.

Snow cover is severely fractured and changes greatly, and there is a large amount of instant snow over the QTP. Therefore, it is difficult to observe continuous snow cover in the entire Water Year. Due to scatterers screening and scanning gap, the single point of meteorological stations cannot cover all the study period, and the time series of single points are discontinuous. The meteorological stations 55437 and 56202 are chosen for time-series analysis with more samples, which are not influenced by scatterers and scanning gap. As shown in Fig. 9, compared with AMSR2 descending SD products, the retrieval model has more accurate results, and its trend accorded with the measured generally. The model has shortcoming retrieved accurately the SD, which is greater than 30 cm, which has a more exact result when the SD is less than 30 cm.

When the ground measured SD is less than 10 cm, the RMSE, MAE, and BIAS for the M8 model have much better performance than the AMSR2 descending SD product (see Table VIII). The AMSR2 descending SD product has poor accuracy when the ground measured SD is greater than 20 cm. The SD inversion model of this study is superior to the official SD product for any interval of actual SD, and the accuracy for areas of shallow snow (SD $<$ 10 cm) also improved.

The average ground emissivity was obtained by the method, which retrieved from [30] (see Fig. 10). The average ground emissivity of each frequency is generally high in the East and low in the West, and the horizontal channels of 10 and 23 GHz are particularly obvious. Moreover, the vertical channels of 23 and 89 GHz have higher emissivity in western plateau than the

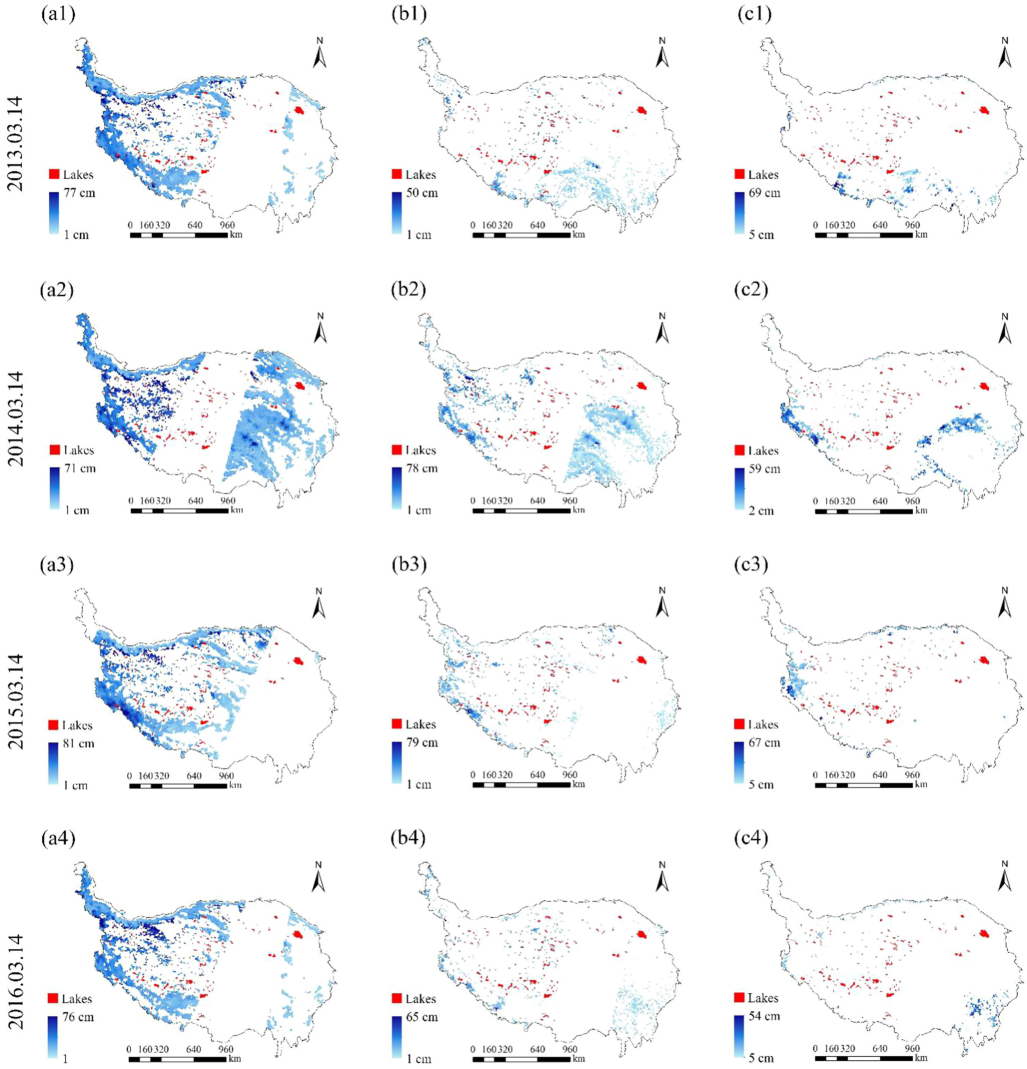

Fig. 8. SD maps of March 14 for each month on March 14 during the period of 2013 and 2016. (a1)–(a4) SD maps of the M8 model. (b1)–(b4) SD maps extracted by MODIS cloud-free snow cover products from M8 model. (c1)–(c4) SD maps of AMSR2 descending products. The blank areas are the snow-free covered and scanning gap.

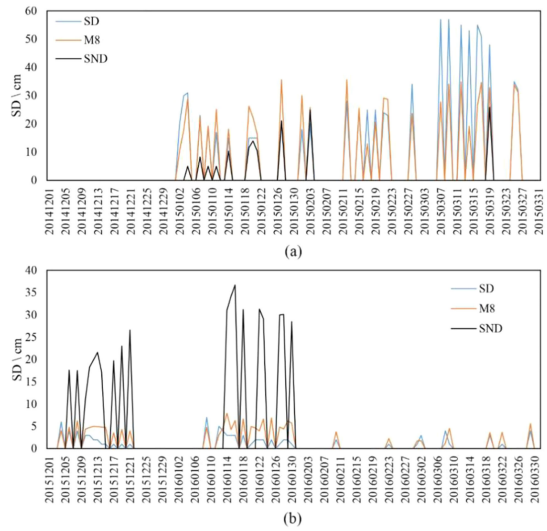

Fig. 9. Time series of (a) 55437 and (b) 56202, where SD, M8, and SND are measured SD, retrieved SD, and AMSR2 SD products, respectively.

horizontal channel of 10 and 23 GHz. The higher emissivity of the eastern QTP has lower inversion error, and the SD inversion error was lower in the region with increased emissivity. The low emissivity areas were most areas that near the water body and bare lands with high altitude, and those areas were less meteorological stations distributed with less measured SD data, which led to worse results. The lakes in the western part of the QTP are densely distributed. However, the high permittivity of water and resulted low emissivity for lake has a much stronger and more direct influence that can result in low emissivity than the water vapor. As a result, the water body in this area affect the radiation transmission of microwaves, which indirectly affect the SD inversion.

V. Discussion

AMSR2 currently provides the most up-to-date passive microwave remote sensing data and has been widely used to monitor snow cover. Research on snow cover is an essential part of

TABLE VIII
COMPARISON OF ACCURACY BETWEEN THE OPTIMAL MODEL AND AMSR2 DESCENDING PRODUCT FOR DIFFERENT SDS

Ground measurements	M8			AMSR2 snow product		
	RMSE (cm)	MAE (cm)	BIAS (cm)	RMSE (cm)	MAE (cm)	BIAS (cm)
≤ 10 cm	4.11	2.59	–0.94	7.67	4.64	–1.57
10 – 20 cm	8.08	6.94	0.92	12.11	10.88	8.24
20 – 30 cm	7.82	6.38	2.72	21.91	20.11	19.28
30 – 40 cm	11.60	9.27	9.21	30.80	29.80	29.80
> 40 cm	22.15	20.59	20.59	40.86	39.78	39.78

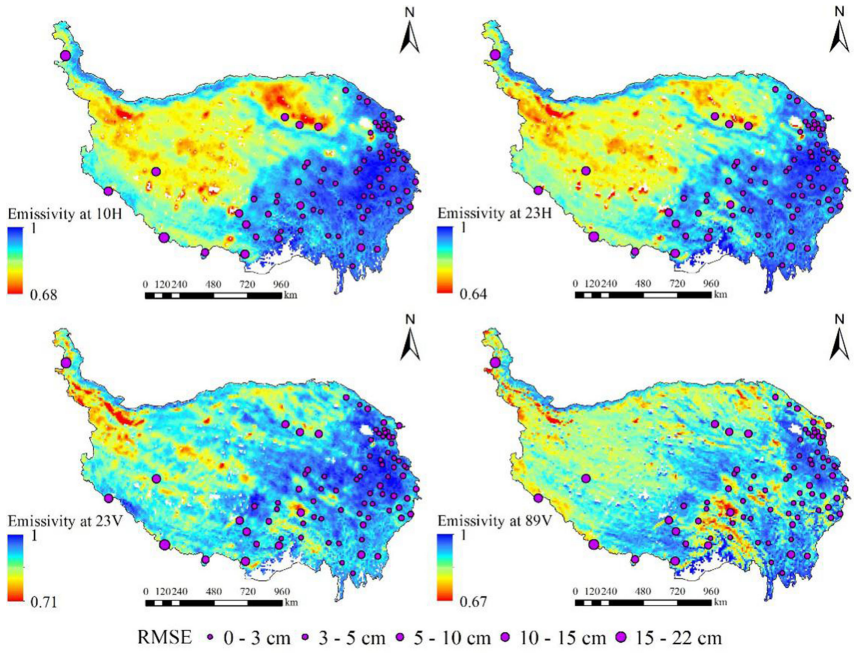

Fig. 10. Effects of varied emissivity in SD inversion over the QTP.

regional climate change. The QTP is an important snow-covered area in China and plays a vital role in global climate change research. The difference in the spatial distribution of SD is large over the QTP, as is the interannual difference. In most areas of the QTP, the SD is shallow and severely fragmented, and most of the snow cover is distributed in high-elevation mountainous areas. For the QTP, with its complex terrain and shallow snow cover, using only the brightness temperature differences to the SD inversion provides an incremental improvement in the inversion results. In previous algorithms such as the Chang algorithm and other various algorithms, the difference in brightness temperature between 18 GHz (or 19 GHz) and 36 GHz was used to establish an SD inversion model. The elevation and longitude were combined with the brightness temperature differences between the high-frequency channel (89 GHz) and the medium–low-frequency channel (10 and 23 GHz) to construct a multiparameter inversion model in this article. The introduction of elevation and longitude improved the accuracy of the SD inversion model over the QTP. The additions of the high-frequency channel (89 GHz) and the medium–low-frequency channel (10 and 23 GHz) are beneficial for improving the inversion accuracy of SD over the QTP. The SD data from the ground meteorological stations were analyzed, which indicated that the measured SD was less than or equal to 5 and 10 cm in approximately 85% and 93% of all study periods, respectively. This result shows that the average SDs at the meteorological stations are shallow in most parts of the QTP during the study period; thus, 89 GHz was added to invert shallow snow cover in this article, which improves the inversion results. At the same time, 23 GHz was added to the SD inversion model, which improved the accuracy of the model to a certain extent. When the snow cover exceeds a certain depth, a saturation phenomenon in the brightness temperature differences between 89 and 23 GHz (or 10 GHz) may also occur.

From southeast to northwest, the land cover type on the QTP gradually changes from forest to grassland, and the elevation roughly increases from East to West. Grassland is a low-height vegetation cover, and it has less radiation to microwaves. Moreover, grasslands are the main-land cover type over the QTP, and its inversion results are the best. The ground meteorological stations over bare lands represent only 2.3% of the meteorological stations throughout the QTP, but the bare lands account for nearly 30% of the QTP. It can be seen that the ground-measured data of the bare lands are scarce, resulting in a slightly large inversion error in the bare lands. Moreover, there is also a wide range of cold desert in bare lands. This inconsistency is the main reason for the poor accuracy of SD inversion in bare lands.

The Himalayas on the QTP is the main area, where the snow cover is thick, and the ground meteorological stations in this area are mainly distributed in the lower valleys, which decreases the accuracy of SD inversion. This result is also consistent with the results of Jiang *et al.* [23]. The inversion errors of the models are large in the western parts of the QTP due to the shortage of ground meteorological stations, while the inversion errors are small in the rest of the QTP. Most of the meteorological stations in the mid-west have an SD greater than 30 cm, but there are few stations in this area, which results in large errors. Moreover, the mid-west parts of QTP are inaccessible and have poor transportation, which results in limited data acquisition capacity in these areas and leads to large prediction errors in this area. Furthermore, the many lakes that are distributed throughout the western QTP have a certain effect on the SD inversion in these areas. Because the SD data affected by a body of water was not used for SD inversion, even less SD data were available in this area. The varied ground emissivity of western QTP affects inversion results indirectly, especially in the areas that distributed lake densely, and these areas with low ground emissivity mislead the snow-covered areas identification. At the same time, these areas distributed extensive cold desert and frozen ground, and it will strongly affect SD inversion in these areas.

Based on the above analysis, the SD inversion model developed in this article is applicable to most parts of the QTP. However, the SD inversion model also has limitations in inverting the SD in areas with thick snow cover and bare lands over the QTP. Therefore, the main approach to improve the accuracy of SD inversion over the QTP is strengthening the acquisition of ground data in the absence of improved meteorological station distribution.

VI. Conclusion

In this article, we used the data from the meteorological stations over the QTP (SD, elevation, and longitude) and AMSR2 passive microwave data to establish a multiparameter linear model of SD inversion. Moreover, the accuracy of the AMSR2 SD product over the QTP was evaluated. The AMSR2 SD product and land cover type data were also used as auxiliary data to evaluate the accuracy of a novel model. Through statistical analysis, the following conclusions are drawn.

1) The SD inversion model established in this article achieves more accurate over the QTP, and the accuracy is significantly improved compared with the accuracy of the descending AMSR2 SD product. The RMSEs of the optimal model and the descending AMSR2 SD product are 5.31 and 13.34 cm, respectively, and the MAEs are 3.29 and 7.26 cm, respectively.
2) The average SD is only 5.30 cm over the four snow seasons due to the shallow snow cover over the QTP. The addition of 10, 23, and 89 GHz as well as elevation and longitude effectively improved the accuracy of the SD inversion model.
3) Elevation, longitude, and land cover type are the main factors affecting SD inversion. The higher the elevation, the worse the accuracy of the SD inversion model. The accuracy of the inversion model is also poor in the western part and cold desert regions. The main reason for this reduced accuracy is that the shortage of meteorological stations in the high-elevation areas and the western QTP and the existence of a wide range of cold desert areas, which led to the poor accuracy of the SD model. Increasing the distribution of ground observation stations in these areas is an effective method to improve the accuracy of the SD inversion model for the QTP.

References

[1] L. Y. Dai, C. Tao, W. Jian, and Z. Pu, "Snow depth and snow water equivalent estimation from AMSR-E data based on a priori snow characteristics in Xinjiang, China (EI)," *Remote Sens. Environ.*, vol. 127, pp. 14–29, Dec. 2012.

[2] D. H. Qin, *Introduction to Cryosphere Science* (in Chinese), Beijing, China: Science Press, 2017, pp. 1–7.

[3] D. K. Hall, "Influence of depth hoar on microwave emission from snow in northern Alaska," *Cold Regions Sci. Technol.*, vol. 13, pp. 225–231, Apr. 1987.

[4] J. L. Foster *et al.*, "A blended global snow product using visible, passive microwave and scatterometer satellite data," *Int. J. Remote Sens.*, vol. 32, no. 5, pp. 1371–1395, 2011.

[5] X. G. Yang, D. H. Qin, and X. Qin, "Progress in the study of interaction between ice/snow and atmosphere," (in Chinese), *J. Glaciol. Geocryol.*, vol. 34, no. 2, pp. 392–402, Apr. 2012.

[6] W. Wang, X. Huang, J. Deng, and H. Xie, "Spatio-temporal change of snow cover and its response to climate over the tibetan plateau based on an improved daily cloud-free snow cover product," *Remote Sens.*, vol. 7, no. 1, pp. 169–194, Jan. 2014.

[7] T. Che and X. Li, "Retrieval of snow depth in China by passive microwave remote sensing data and its accuracy assessment," (in Chinese), *Remote Sens. Technol. Appl.*, vol. 26, no. 4, pp. 444–449, Jun. 2004.

[8] T. Che, X. Li, and F. Gao, "Estimation of snow water equivalent in the Tibetan plateau using passive microwave remote sensing data (SSM/I)," (in Chinese), *J. Glaciol. Geocryol.*, vol. 26, no. 3, pp. 363–368, Oct. 2004.

[9] Y. Zhang, S. Wang, A. G. Barr, and T. A. Black, "Impact of snow cover on soil temperature and its simulation in a boreal aspen forest," *Cold Regions Sci. Technol.*, vol. 52, no. 3, pp. 355–370, May 2008.

[10] M. Tedesco and P. S. Narvekar, "Assessment of the NASA AMSR-E SWE product," *IEEE J. Sel. Topics Appl. Earth Observ. Remote Sens.*, vol. 3, no. 1, pp. 141–159, Mar. 2010.

[11] B. T. Pan and J. J. Li, "Qinghai–Tibetan Plateau: A driver and amplifier of the global climatic change," (in Chinese), *J. Lanzhou Univ.*, vol. 32, no. 1, pp. 108–115, 1996.

[12] H. Sun, D. Zheng, T. Yao, and Y. Zhang, "Protection and construction of the national ecological security shelter zone on Tibetan Plateau," (in Chinese), *Acta Geograph. Sinica*, vol. 67, no. 1, pp. 3–12, Jan. 2012.

[13] Y. L. Wang *et al.*, "Development and validation for daily cloud-free snow products in middle-and-high latitude areas in Eurasia," *Remote Sens. Technol. Appl.*, vol. 31, no. 5, pp. 1013–1021, May 2016.

[14] J. Dong, J. P. Walker, and P. R. Houser, "Factors affecting remotely sensed snow water equivalent uncertainty," *Remote Sens. Environ.*, vol. 97, no. 1, pp. 68–82, Jul. 2005.

[15] J. Gao, M. W. Williams, X. Fu, and G. Wang, "Spatiotemporal distribution of snow in Eastern Tibet and the response to climate change," *Remote Sens. Environ.*, vol. 121, no. 138, pp. 1–9, Jun. 2012.

[16] M. Tedesco, C. Derksen, J. S. Deems, and J. L. Foster, "Remote sensing of snow depth and snow water equivalent," in *Remote Sensing of the Cryosphere*. Hoboken, NJ, USA: Wiley, 2014, pp. 73–98.

[17] W. F. Xu, L. Ma, M. Ma, H. Zhang, and W. Yuan, "Spatial–temporal variability of snow cover and depth in the Qinghai–Tibetan Plateau," *J. Climate*, vol. 30, no. 4, pp. 1521–1533, Feb. 2015.

[18] Y. S. Zhang and N. Ma, "Spatiotemporal variability of snow cover and snow water equivalent in the last three decades over Eurasia," *J. Hydrol.*, vol. 559, pp. 238–251, Apr. 2018.

[19] J. L. Foster, D. K. Hall, R. Kelly, and L. S. Chiu, "Seasonal snow extent and snow mass in South America using SMMR and SSM/I passive microwave data (1979–2006)," *Remote Sens. Environ.*, vol. 113, no. 2, pp. 291–305, Feb. 2009.

[20] C. Derksen *et al.*, "Development of a tundra-specific snow water equivalent inversion algorithm for satellite passive microwave data," *Remote Sens. Environ.*, vol. 114, no. 8, pp. 1699–1709, Aug. 2010.

[21] T. Che, L. Dai, X. Zheng, X. Li, and K. Zhao, "Estimation of snow depth from passive microwave brightness temperature data in forest regions of northeast China," *Remote Sens. Environ.*, vol. 183, pp. 334–349, Sep. 2016.

[22] M. Sturm, B. Taras, G. E. Liston, C. Derksen, T. Jonas, and J. Lea, "Estimating snow water equivalent using snow depth data and climate classes," *J. Hydrometeorol.*, vol. 11, no. 11, pp. 1380–1394, Aug. 2010.

[23] L. Jiang, P. Wang, L. Zhang, and H. Yang, "Improvement of snow depth inversion for FY3B–MWRI in China," *Sci. China Earth Sci.*, vol. 57, no. 6, pp. 1278–1292, Feb. 2014.

[24] R. P. Zhang *et al.*, "Evaluation and adjustment of the AMSR2 snow depth algorithm for the Northern Xinjiang Region, China," *IEEE J. Sel. Topics Appl. Earth Observ. Remote Sens.*, vol. 10, no. 9, pp. 3892–3903, Sep. 2017.

[25] T. C. Chang, J. L. Foster, and D. K. Hall, "Nimbus–7 SMMR derived global snow cover parameters," *Ann. Glaciol.*, vol. 9, no. 71, pp. 39–44, 1987.

[26] A. T. C. Chang, J. L. Foster, D. K. Hall, D.A. Robinson, L. Peiji, and C. Meisheng, "The use of microwave radiometer data for characterizing snow storage in western China," *Ann. Glaciol.*, vol. 16, pp. 215–219, 1991.

[27] Y. Bo, X. Feng, X. Li, and X. Chen, "The retrieval of snow depth in Qinghai–Xizang (Tibet) plateau from passive microwave remote sensing data and its results assessment," (in Chinese), *J. Remote Sens.*, vol. 5, no. 3, pp. 161–165, 2001.

[28] J. L. Foster, A. T. C. Chang, and D. K. Hall, "Comparison of snow mass estimates from a prototype passive microwave snow algorithm, a revised algorithm and a snow depth climatology," *Remote Sens. Environ.*, vol. 62, no. 2, pp. 132–142, Nov. 1997.

[29] A. B. Tait, "Estimation of snow water equivalent using passive microwave radiation data," *Remote Sens. Environ.*, vol. 64, pp. 286–291, 1998.

[30] L. Dai, T. Che, H. Xie, and X. Wu, "Estimation of snow depth over the Qinghai–Tibetan Plateau based on AMSR-E and MODIS data," *Remote Sens.*, vol. 10, no. 12, Dec. 2018, Art. no. 1989.

[31] M. Pardé, K. Goïta, and A. Royer, "Inversion of a passive microwave snow emission model for water equivalent estimation using airborne and satellite data," *Remote Sens. Environ.*, vol. 111, no. 2, pp. 346–356, Nov. 2007.

[32] M. J. Butt, "A comparative study of Chang and HUT models for UK snow depth retrieval," *Int. J. Remote Sens.*, vol. 30, no. 24, pp. 6361–6379, 2009.

[33] Y. Qiu, H. Guo, C. Bin, D. Chu, L. Shi, and J. Lemmetyinen, "Comparison on snow depth algorithms over China using AMSR–E passive microwave remote sensing," in *Proc. IEEE Geosci. Remote Sens. Symp.*, 2014, pp. 851–854.

[34] M. Cao, P. J. Li, D. A. Robinson, T. E. Spies, and G. Kukla, "Evaluation and primary application of microwave remote sensing SMMR–derived snow cover in western China," (in Chinese), *Remote Sens. Environ., China*, vol. 8, no. 4, pp. 260–269, 1993.

[35] J. Liang *et al.*, "Improved snow depth inversion by integrating microwave brightness temperature and visible/infrared reflectance," *Remote Sens. Environ.*, vol. 156, pp. 500–509, 2015.

[36] J. Wang *et al.*, "Remote sensing for snow hydrology in China: Challenges and perspectives," *J. Appl. Remote Sens.*, vol. 8, no. 25, Jun. 2014, Art. no. 084687.

[37] T. Che, X. Li, R. Jin, R. Armstrong, and T. Zhang, "Snow depth derived from passive microwave remote-sensing data in China," *Ann. Glaciol.*, vol. 49, no. 1, pp. 145–154, 2008.

[38] S. Hancock, R. Baxter, J. Evans, and B. Huntley, "Evaluating global snow water equivalent products for testing land surface models," *Remote Sens. Environ.*, vol. 128, pp. 107–117. Jan. 2013.

[39] K. Luojus *et al.*, "ESA Globsnow: Algorithm theoretical basis document—SWE-algorithm," Eur. Space Agency, Paris, France, Tech. Rep. 21703/08/I-EC, 2013.

[40] T. Smith and B. Bookhagen, "Assessing uncertainty and sensor biases in passive microwave data across high mountain Asia," *Remote Sens. Environ.*, vol. 181, pp. 174–185, Aug. 2016.

[41] R. L. Armstrong and M. J. Brodzik, "Hemispheric-scale comparison and evaluation of passive-microwave snow algorithms," *Ann. Glaciol.*, vol. 34, no. 1, pp. 38–44, 2002.

[42] M. H. Savoie, R. L. Armstrong, M. J. Brodzik, and J. R. Wang, "Atmospheric corrections for improved satellite passive microwave snow cover retrievals over the Tibet Plateau," *Remote Sens. Environ.*, vol. 113, no. 12, pp. 2661–2669, Dec. 2009.

[43] X. Xiao, T. Zhang, X. Zhong, W. Shao, and X. Li, "Support vector regression snow-depth retrieval algorithm using passive microwave remote sensing data," *Remote Sens. Environ.*, vol. 210, pp. 48–64, Jun. 2018.

[44] J. Liang, X. Liu, K. Huang, and X. Li, "Improved snow depth retrieval by combining SSMI and MODIS data," in *Proc. AGU Fall Meeting Abstr.*, 2013.

[45] R. Kelly, "The AMSR-E snow depth algorithm: Description and initial results," *J. Remote Sens. Soc. Japan*, vol. 29, no. 1, pp. 307–317, 2009.

[46] Y. Yao and B. Zhang, "The spatial pattern of monthly air temperature of the Tibetan Plateau and its implications for the geo-ecology pattern of the Plateau," (in Chinese), *Geograph. Res.*, vol. 34, no. 11, pp. 2084–2094, Nov. 2015.

[47] S. Y. Bai, J. Q. Shi, and J. X. Gao, "Analysis of spatial–temporal variations of snow depth over the Qinghai–Tibetan Plateau during 1979–2010," (in Chinese), *J. Geo–Inf. Sci.*, vol. 16, no. 4, pp. 628–637, Apr. 2014.

[48] S. Bai *et al.*, "Spatial–temporal variation of snow depth in Tibet and its response to climatic change in the past 30 years," (in Chinese), *Remote Sens. Land Resources*, vol. 26, no. 1, pp. 144–151, 2014.

[49] T. C. Chang, J. L. Foster, and D. K. Hall, "Effects of forest on the snow parameters derived from microwave measurements during the Boreas winter field campaign," *Hydrol. Processes*, vol. 10, pp. 1565–1574, Dec. 1996.

[50] N. C. Grody, "Classification of snow cover and precipitation using the special sensor microwave imager," *J. Geophys. Res. Atmosp.*, vol. 96, no. D4, pp. 7423–7435, Apr. 1991.

[51] E. Walker, and B. E. Goodison, "Discrimination of a wet snow cover using passive microwave satellite data," *Ann. Glaciol.*, vol. 17, pp. 307–311, Jan. 1993.

[52] N. C. Grody and A. N. Basist, "Global identification of snowcover using SSM/I measurements," *IEEE Trans. Geosci. Remote Sens.*, vol. 34, no. 1, pp. 237–249, Jan. 1996.

[53] C. Mätzler, "Passive microwave signatures of landscapes in winter," *Meteorol. Atmos. Phys.*, vol. 54, nos. 1–4, pp. 241–260, 1994.

[54] J. Tennant *et al.*, "Regional sensitivities of seasonal snowpack to elevation, aspect, and vegetation cover in western North America," *Water Resources Res.*, vol. 53, no. 8, pp. 6980–6926, Aug. 2017.

[55] Y. He and Y. Bo, "A consistency analysis of MODIS MCD12Q1 and MERIS Globcover land cover datasets over China," in *Proc. Int. Conf. Geoinform.*, 2011, pp. 1–6.

[56] Y. L. Wang, X. D. Huang, H. Liang, Y. H. Sun, Q. F. Feng, and T. G. Liang, "Tracking snow variations in the northern hemisphere using multi-source remote sensing data (2000–2015)," *Remote Sens.*, vol. 10, no. 1, Jan. 2018, Art. no. 136.

[57] T. Markus, D. C. Powell, and J. R. Wang, "Sensitivity of passive microwave snow depth inversions to weather effects and snow evolution," *IEEE Trans. Geosci. Remote Sens.*, vol. 44, no. 1, pp. 68–77, Feb. 2006.

[58] X. Zhang *et al.*, "Snow parameter estimation from microwave remote sensing data," (in Chinese), *Mountain Res.*, vol. 32, no. 3, pp. 307–313, May 2014.

[59] Y. Bi, H. Xie, C. Huang, and C. Ke, "Snow cover variations and controlling factors at upper Heihe River Basin, Northwestern China," *Remote Sens.*, vol. 7, no. 6, pp. 6741–6762, Jun. 2015.

[60] H. Li, Y. He, X. Hao, T. Che, J. Wang, and X. Huang, "Downscaling snow cover fraction data in mountainous regions based on simulated inhomogeneous snow ablation," *Remote Sens.*, vol. 7, no. 7, pp. 8995–9019, Jul. 2015.

[61] W. D. Berry, *Linear Regression Analysis Basis* (in Chinese). Shanghai, China: Shanghai People's Publishing House, 2011.

[62] Z. Sun *et al.*, "Progress in study of snow parameter inversion by passive microwave remote sensing," (in Chinese), *Remote Sens. Land Resources*, vol. 27, no. 1, pp. 9–15, Mar. 2015.
[63] Y. Liu, J. W. Bi, and Z. P. Fan, "Multi-class sentiment classification: The experimental comparisons of feature selection and machine learning algorithms," *Expert Syst. Appl.*, vol. 80, pp. 323–339, Sep. 2017.

Jianshun Wang received the Bachelor of Agriculture degree in grassland science, in 2017 from Gansu Agricultural University, Lanzhou, China. He is currently working toward the M.S. degree in grassland science with Lanzhou University, Lanzhou.

His current research interests include remote sensing on snow, snow depth inversion, and modeling.

Xiaodong Huang received the B.S. degree in geographic information systems and the Ph.D. degree in grassland science from Lanzhou University, Lanzhou, China, in 2004 and 2009, respectively.

He is currently a Professor with the School of Geographical Sciences, Nanjing University of Information Science and Technology, Nanjing, China. His research interests include snow cover monitoring using remote sensing technology. His research interests also include surface hydrology, agriculture, and environment studies.

Yunlong Wang received the Bachelor of Agriculture degree in grassland science from Gansu Agricultural University, Lanzhou, China, in 2015. He is currently working toward the Ph.D. degree in grassland science with Lanzhou University, Lanzhou.

His current research interests include remote sensing of snow, climate change, and geographic information system applications on cryosphere.

Tiangang Liang received the B.S. and M.S. degrees in geographic information systems from Lanzhou University, Lanzhou, China, in 1989 and 1992, respectively, and the Ph.D. degree in ecology from the State Key Laboratory of Arid Agroecology, Lanzhou University, in 1998.

He is currently a Professor with the College of Pastoral Agriculture Science and Technology, Lanzhou University, where he is also the Director of the Institute of Grassland Remote Sensing and Geographic Information System. His research interests include remote sensing and geographic information system technologies, theories, and applications on grassland ecology and environment.